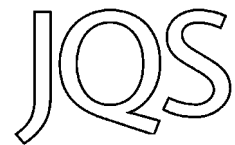


Glacially derived material in an Inner Mongolian desert lake during Marine Isotope Stage 2



KANDASAMY SELVARAJ,^{1,2,3} CHEN-TUNG ARTHUR CHEN,^{3*} C. PRAKASH BABU,^{3,4}
JIANN-YUH LOU,⁵ CHING-LING LIU³ and KENNETH J. HSU⁶

¹State Key Laboratory of Marine Environmental Science, Xiamen University, Xiamen, China

²Research Center for Environmental Changes, Academia Sinica, Taipei, Taiwan

³Institute of Marine Geology and Chemistry, National Sun Yat-sen University, Kaohsiung, Taiwan

⁴Geological Oceanography Division, National Institute of Oceanography, Dona Paula, Goa, India

⁵Department of Marine Science, Naval Academy, Tsoying, Kaohsiung, Taiwan

⁶Tarim Resources Recycling Company, Haslemere, UK

Received 29 April 2012; Accepted 12 May 2012

ABSTRACT: Establishing the precise timing of continental glacial dynamics and abrupt high-latitude climate events is crucial to understanding the causes of global climate change. Here we present multi-proxy records in a lake sediment core from arid Inner Mongolia (Wuliangshuai Lake) that show two distinct glacially derived sedimentation events at ~26.2–21.8 and ~17.3–11.5k cal a BP. Fine sediments from the Last Glacial Maximum separate these glacially derived coarse sediments. Within these intervals, the occurrence of granite clasts at ~24–23.5, 17.3–17 and 15.6–14.1k cal a BP implies either sediment discharge by meltwater as well as strong current flow in the Yellow River and/or sediment influx through hill-slope mass wasting and landsliding from the nearby Yin Mountains. Surface microfeatures of quartz grains and spot elemental analysis of black specks in these intervals, however, indicate that physical weathering is dominant and that the provenance of the rocks is probably from a glacial source. To the best of our knowledge, this is the first time glacier-derived materials have been detected in any desert lake in the Yellow River basin. The occurrence of granite clasts roughly correlates with Heinrich events in the North Atlantic, suggesting synchronous ice sheet dynamics in high- and mid-latitude regions during the Last Glacial period. Although our data provide unprecedented evidence for the influence of glacier-related processes in arid Inner Mongolia, further well-dated records are clearly needed to re-evaluate the correlative inference drawn between granite clast layers in Wuliangshuai Lake and Heinrich events in the North Atlantic. Copyright © 2012 John Wiley & Sons, Ltd.

KEYWORDS: glacially derived sediments; Inner Mongolia; Last Glacial period; mountain glaciation; Wuliangshuai Lake; Yellow River.

Introduction

Climatic transitions associated with winter and summer monsoons in Asia are recorded as loess–palaeosol alternations in central China, and these sedimentary transitions are consistent with changing oceanic conditions in the North Atlantic and air temperatures over Greenland (Porter and An, 1995; An and Porter, 1997; Ruth *et al.*, 2007). This dual behaviour of Asian monsoons greatly influences climate in central Asia, where high mountains experience glacial advances and retreats asynchronous with high-latitude glaciations during the Last Glacial period (Gillespie and Molnar, 1995). Glacial deposits such as moraines and tills provide an excellent record of mountain glaciation during the late Quaternary (Gillespie and Molnar, 1995; Owen *et al.*, 2002; Shi, 2002). Glacier-derived sediments, including moraines, are formed by glacial advance and retreat, can reflect variations in temperature and precipitation (Denton *et al.*, 1999) and can therefore demarcate and define glaciation events and contemporaneous periglacial and paraglacial processes in plain regions adjoining mountain ranges (Vandenberghe *et al.*, 2004). Lakes connected to rivers discharging from mountain glaciers are therefore affected by regional and global climate changes, including monsoon variability. The Yellow River originates in the Qinghai–Tibetan plateau where extensive glacial advances have been reported (Shi, 1992). However, the impact of mountain glaciers on river discharge into the desert lakes and their high-latitude teleconnection during the Last

Glacial period remain poorly understood. Here we describe, for the first time, glacially derived materials, including macroscopic granite clasts and glacial microfeatures on quartz grains, in the sediments of an arid Inner Mongolian lake. These sediments serve as a palaeoclimate archive documenting various processes, including fluvial, aeolian, mass wasting and glacial dynamics on the Qinghai–Tibetan plateau, that are responsible for sediment sources in cold and arid regions of China.

Study area

The Hetao basin is one of the Cenozoic fault-bounded rift basins in central China (Figs 1 and 2), where the sedimentary environment, palaeogeography and lithology have been affected by both palaeoclimate and tectonic movement (Guo *et al.*, 2008). During the Quaternary, inland lacustrine fine-grained sediments were deposited locally and a thick mid-Cenozoic sedimentary formation has developed in the basin. Quaternary sediments are mostly sourced from the Langshan Mountains and partly from fluvial deposits of the Yellow River, which are dominated by sand, silt and clay. The fluvial sediments originating from the old Yellow River were mainly deposited in the southern part of Hetao basin, whereas alluvial and pluvial sediments dominate in the northern part. Quaternary sediments in the basin are up to 200–1500 m thick, but the sediments are thinner (about 20–50 m) near the forefront of Yin Mountains (Fig. 1). In central China, the modern Yellow River flows northward into the arid Hetao Plain, bends eastward around the Ordos Plateau and then turns south to form 'the Great Bend' (Figs 1 and 2). During the Last Glacial period, the river drained directly into a Jilantai–Hetao

*Correspondence: C.-T. A. Chen, as above.

E-mail: ctchen@mail.nsysu.edu.tw

Re-use of this article is permitted in accordance with the terms and conditions set out at http://wileyonlinelibrary.com/onlineopen#OnlineOpen_Terms

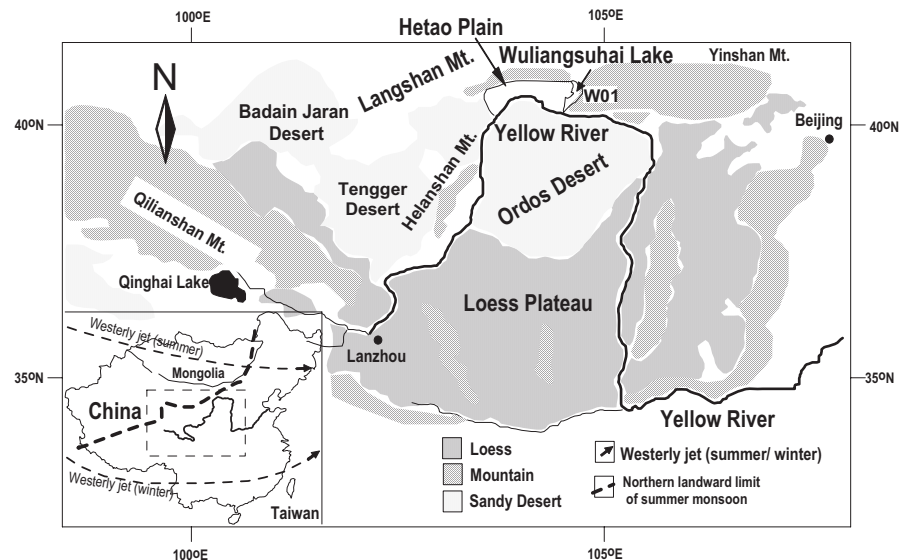


Figure 1. Location of core WO-1 in Inner Mongolia and the surrounding mountains, deserts and the central Loess Plateau. Inset: the northern boundary of the East Asian summer monsoon (thick dashed line) and the positions of westerly jets (thin dashed line) during summer and winter.

Megalake on the northern side of the Great Bend, where extensive fluvial sediments were deposited (Chen *et al.*, 2008). Optical dating of quartz grains reveals the lake formed before ~60–50 ka, and four periods of lake level changes occurred between 1060 and 1035 m above sea level from ~60 ka to the early Holocene (Chen *et al.*, 2008).

The study area, Wuliangshuai Lake (40°36′–41°03′N, 108°43′–108°57′E) is located on the western end of Hetao Plain in arid Inner Mongolia (Figs 1 and 2). A recent study based on geographical map data, remote sensing, historical documentation and field observations has suggested that the north-river located at the south side of the Langshan Mountains was the mainstream of the Yellow River (Figs 1 and 2), flowing to the east (Sun *et al.*, 2011). Continuous uplift of the Yin Mountains due to tectonic uplift blocked the northern branch of the Yellow River, sharply reversing the flow southward, leading to outflow out of a large depression, the predecessor of Wuliangshuai Lake. Subsequent wind erosion of sand continually expanded an alluvial fan south of the Langshan Mountains, which also resulted in a riverbed raise. The combination of these processes led to the riverbed of north-river filling with sediments, forming the Wuliangshuai Lake as a river terrace lake, which developed over the pediment in front of the steep southerly sloping Yin

Mountains (Chen *et al.*, 2008; Sun *et al.*, 2011). This crescent-shaped, shallow (0.5–2.5 m water depth), open, low-latitude (1017 m) freshwater lake is the largest lake within the reaches of the Yellow River (total area ~290 km²); the region surrounding the lake experiences a wide range of temperatures (max. 37.7°C; min. –30.8°C) with an annual mean of 7.3°C. As the lake is situated close to the northern landward limit of the present-day East Asian summer monsoon (Fig. 1), it receives a low mean annual rainfall of 224 mm, while the evaporation rate is nearly seven-fold higher at 1500 mm.

Materials and methods

Here we focus our study on a 20.7-m-long sediment drill core, WO-1, raised from Wuliangshuai Lake (40°58′04.60″N, 108°54′46.55″E). Visual observations of the core prior to sub-sampling identified two stratigraphically distinct gravel strata at depth intervals of ~1130–1390 and 420–830 cm (Supporting information, Figs S1 and S2). Numerous oversized pink granite clasts located intermittently in these intervals are attributed to glacial erosion/abrasion and imply the presence of glacially derived materials in the lake. Magnetic susceptibility (MS) provides evidence for the timing of glaciation (Benson *et al.*, 1996) and thus can be used as a proxy for glacial erosion. In general, sediment MS values depend upon three variables (Reynolds *et al.*, 2004): (i) the sediment mineral composition, (ii) the flux of magnetic and non-magnetic (e.g. quartz) minerals and (iii) biogenic minerals (e.g. carbonates). The MS value of sediment therefore increases with increasing magnetic mineral content and flux and with decreasing biogenic minerals. Correlation between high sediment MS values and glacial periods has been well established in a number of marine and lake settings (e.g. Bard *et al.*, 2000; Reynolds *et al.*, 2004; Tripathi *et al.*, 2008). For example, in the North Atlantic, periods of intense ice-rafting called Heinrich events are identified by the increased MS peaks and oversized lithic grains in a number of marine sediment cores (Heinrich, 1988; Bond *et al.*, 1993). Bard *et al.* (2000) used the ice-rafted detritus (IRD) counts and MS record to identify detrital sedimentation formed by Heinrich events in the mid-latitude Iberian continental margin. Therefore, to delineate glacially derived sedimentation and determine their likely provenance, we measured mass MS and grain size, including the gravel content, and generated major and trace element data for the length of the core, given

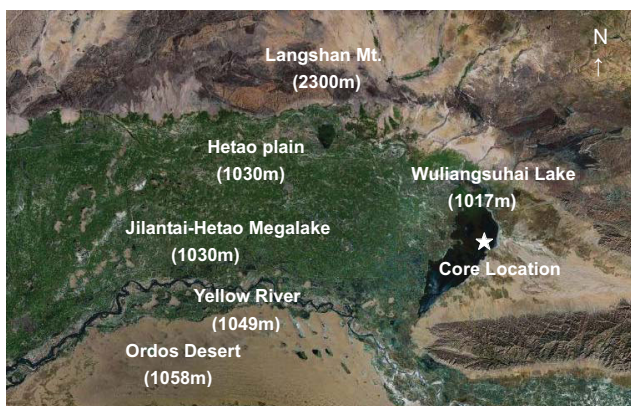


Figure 2. Satellite image showing the core location, Hetao Plain, Yellow River and surrounding mountains and deserts. Numbers in parentheses indicate the altitudes of the locations. This figure is available in colour online at wileyonlinelibrary.com.

that physical weathering dominance under cold climate would usually produce geochemical elements in sediments that are very similar to the composition of source rocks. Although we did not measure MS or other geochemical parameters on background materials in the catchment, we deem that our multi-proxy records and their distinct behaviours from each interval of the core are sufficient to support the interpretations made in this preliminary report.

Drill core WO-1 retrieved from the lake was sub-sampled at 0.5- and 1-cm intervals for magnetic, grain size and geochemical studies. Samples were freeze-dried and gently broken apart using a pestle and mortar. Hydrogen peroxide (30%) solution was added to a portion of each subsample to remove organic matter. Once diluted, 10% hydrochloric acid was then added to remove carbonate. The remaining residue was sieved at 2 and 1 mm, and weighed as gravel (>2 mm) and very coarse sand (>1 mm). The grain sizes of the <1-mm sediment fractions were determined using a Coulter LS-230 laser particle size analyser. Fine resolution (3–47 years) MS measurements were made at 0.5-, 1- and 2-cm intervals using a Bartington Instruments' MS2B dual-frequency MS meter.

For elemental analysis, the sub-samples of bulk sediments (<2 mm) were oven dried at 60 °C, finely powdered (~200 mesh) and homogenized by using agate mortar. Total carbon (TC) was determined with a LECO CHN-932 elemental analyser. After liberating CO₂ with 1 M hydrochloric acid, inorganic carbon (IC) was measured with a CM 5011 UIC Coulometer. Analytical accuracy and precision of the two methods were better than 5%. Total organic carbon (TOC) content was calculated as the difference between TC and IC and the content of IC was converted to calcium carbonate (CaCO₃) by multiplying by 8.333. For geochemical analysis, a round disc pellet (30 mm diameter) was made from 2–3 g of powdered sediment under appropriate pressure with cellulose as a backing material. The concentration of selected major (Si, Ti, Al, Fe, Ca, Mg, Na and K) and trace elements (Ba, Rb and Sr) were determined by X-ray fluorescence spectroscopy on a Rigaku RIX 2000 system equipped with Rh tube. In addition, a granite rock piece found at depths of ~574–580 cm was also analysed for major and trace elements for comparison. The measurements were carried out at an acceleration voltage of 50 kV and a current of 50 mA. Seven international reference materials, namely BCSS-1, MESS-1, PACS-1, MAG-1, NIES-2, SRM-2707 and GBW-07314, were used for calibration. Replicate analyses of the samples gave a precision of ±2%

for major elements and ±5% for trace elements. The elemental analyses were carried out regularly at 10-cm intervals.

To identify the provenance of detrital material, three samples from glacially derived sedimentation events at depths of 530, 550 and 1280 cm were selected for scanning electron microscopy (SEM) observations. The granular sediment samples were allowed to pass through a 0.300-mm sieve and those retained on a 0.177-mm sieve were boiled in concentrated hydrochloric acid for 10 min, washed thoroughly with distilled water, and boiled again with a few drops of stannous chloride solution to remove iron oxide coatings. The stain-free samples were viewed under a Hitachi S-3000 N SEM instrument. For SEM-EDX (SEM-energy dispersive X-ray) study, the magnetic particles from three depth intervals at 550–570, 750–760 and 1240–1250 cm were separated with a hand-held magnet and spot elemental analysis was carried out semi-quantitatively.

Results

Chronology and lithostratigraphy

Twelve ¹⁴C accelerator mass spectrometer (¹⁴C-AMS) dates on TOC were obtained at Leibniz-Labor Laboratory, Germany (KIA) and Rafter Radiocarbon Laboratory, New Zealand (NZA) (Table 1). Only nine dates were used for age modelling (Fig. 3) because not all ¹⁴C dates were in stratigraphic sequence. For instance, the ¹⁴C age of sediment TOC at 12 cm shows an older age (7030 ± 30 ¹⁴C a BP) with low percentage modern carbon (pMC; 41.68 ± 0.18) compared with TOC at relatively deeper depths (80, 120 and 200 cm). Sediment at 360 cm was dated both for alkali and for humic fractions of TOC. The age difference between these two measurements is 900 ¹⁴C a, implying the heterogeneous nature of organic carbon in the top section of the core. ¹⁴C measurements on TOC include highly mobile components belonging to the fulvic acid and less mobile humic acid fractions as well as components of older reworked organics. This mixture of organics of different ages and origins may be responsible for age scattering. Additionally, the section with more aeolian sediment contains older, reworked material increasing towards the present. At a depth of 680 cm, the ¹⁴C date of 3770 ± 25 a BP with high pMC (58.05 ± 0.27) is significantly younger than the dates at relatively shallower depths (628 and 200 cm; also see supporting Appendix S1: Chronology). These three dates were

Table 1. Details of accelerator mass spectrometry radiocarbon (¹⁴C) dates in core WO-1.

| Lab. code | Core depth (cm) | Dating material | Age (¹⁴ C a) | Age (1σ) (cal a BP)* † | Age (cal a BP) | TOC (%) | δ ¹³ C (‰) |
|------------|-----------------|-----------------|--------------------------|------------------------|----------------|---------|-----------------------|
| KIA-32843‡ | 12 | TOC | 7030 ± 35 | 7840–7920 | 5930 ± 40 | 1.92 | –28.68 ± 0.16 |
| KIA-32844 | 80 | TOC | 3500 ± 25 | 3730–3820 | 3780 ± 40 | 0.72 | –23.78 ± 0.10 |
| KIA-30806 | 120 | TOC-alkali | 4835 ± 60 | 5495–5630 | 5560 ± 70 | 0.65 | –26.29 ± 0.24 |
| KIA-30807 | 200 | TOC-alkali | 5660 ± 70 | 6370–6540 | 6450 ± 90 | 0.20 | –25.66 ± 0.24 |
| KIA-30808‡ | 360 | TOC-alkali | 4370 ± 40 | 4890–5010 | 4850 ± 60 | 0.22 | –23.90 ± 0.16 |
| | 360 | TOC-humic | 3470 ± 50 | 3680–3820 | 3750 ± 70 | 0.22 | –25.32 ± 0.12 |
| NZA-7857 | 628 | TOC | 13 385 ± 60 | 15 910–16 740 | 16 330 ± 400 | 0.20 | –24.30 |
| KIA-32846‡ | 680 | TOC | 3770 ± 25 | 4100–4205 | 4155 ± 50 | 0.19 | –23.65 ± 0.10 |
| NZA-7888 | 874 | TOC | 14 387 ± 87 | 17 280–17 800 | 17 540 ± 260 | 0.06 | –21.90 |
| NZA-7914 | 1458 | TOC | 22 620 ± 60 | 26 970–27 720 | 27 350 ± 370 | 2.04 | –23.40 |
| KIA-32847 | 1549 | TOC | 23 630 ± 160 | 28 170–28 980 | 28 570 ± 400 | 0.72 | –22.73 ± 0.32 |
| | 1549 | TOC§ | 24 570 ± 290 | 28 210–29 970 | 29 400 ± 580 | 0.72 | –23.63 ± 0.12 |
| NZA-7858 | 1790 | TOC | 25 400 ± 190 | 29 930–30 580 | 30 250 ± 320 | 0.43 | –24.60 |
| KIA-32848 | 1971 | TOC | 32 070 ± 480 | 35 600–37 380 | 36 490 ± 890 | 0.34 | –24.25 ± 0.12 |

* Calib 4.1 (Stuiver *et al.*, 1998). † CalPal^{online} calibration. ‡ Dates not used for age model reconstruction. § The combustion of TOC at 1000 °C for 8 h instead of normal combustion of TOC at 800 °C for 4 h. KIA, lab code for Leibniz-Labor Laboratory, Germany; NZA, lab code for Rafter Radiocarbon Laboratory, New Zealand.

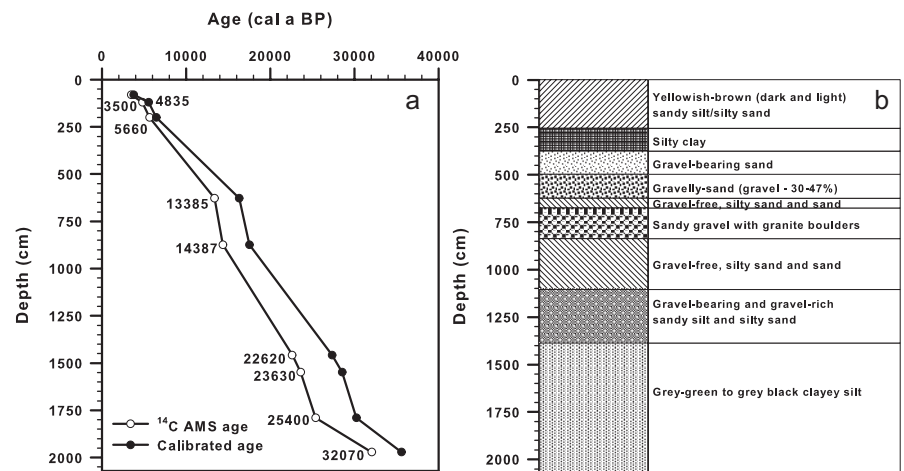


Figure 3. Depth versus age (a) and sediment stratigraphy (b) of core WO-1.

thus rejected (Table 1) and the remaining nine dates were converted to calendar years before the present (cal a BP) to derive the age model (Stuvier *et al.*, 1998; Danzeglocke *et al.*, 2008). Continuous time series were established by linear interpolation between each pair of calibrated ^{14}C dates, with the basal age of the core identified as $\sim 40\text{k}$ cal a (40 000 calendar years) BP.

The core consists primarily of siliciclastic sediments dominated by gravel, sand and silt with a significant amount of clay (max. 27%, Fig. 3, supporting Table S1). Based on the sediment stratigraphy, chronology and grain size data, we divided core WO-1 into three climatically controlled depositional units (Figs 3, 4, and supporting Figs S1 and S2): (i) laminated grey green to grey black clayey silt (77–99%) sediments deposited at ~ 2070 and 1390 cm, representing the majority of Marine Isotope Stage 3 (MIS 3) (~ 40 – 26.2k cal a BP); (ii) detrital materials consisting of coarse sand, gravel and macroscopic granite clasts deposited between 1390 and 380 cm, denoting sedimentation induced by mountain glaciation-driven and/or hill-slope processes during MIS 2 (26.2–10.6k cal a BP); and (iii) sediments dominated by fine sand and loess materials deposited above ~ 380 cm, designating MIS 1 or the Holocene (10.6k cal a BP to the present). Mean sedimentation rates are about 36, 65 and 49 cm ka^{-1} in MIS 1, 2 and 3, although granite clasts layers show even higher sedimentation rates.

The dominance of detrital sediments during MIS 2 reveals that the lake was well connected to the Yellow River. Compared with sediments of MIS 3 and 1, very low contents of TOC (0.02–0.48%) and CaCO_3 (1.08–8.58%; Fig. 5) in sediments of MIS 2, suggested sparse vegetation surrounding the lake and decreased water column temperatures, respectively, probably due to cold climatic conditions and perhaps meltwater discharge into the lake. Furthermore, detrital gravel and sand dominate the layers identified as being glacially derived and thus not dominated by carbonate materials (e.g. limestone) compared with CaCO_3 content in other intervals, i.e. MIS 3 and 1. This indicates that input of limestone or other carbonate rocks into Wuliangshai Lake was either a minimum or insignificantly affected MS values, at least in sediments of MIS 2.

Glacial events and granite clasts

Depth profiles of MS, mean grain size, and gravel and sand contents in core WO-1 show two detrital glacially derived sedimentation (G) events at ~ 1390 – 1130 cm (~ 26.2 – 21.8k cal a BP; G2) and ~ 830 – 420 cm (17.3 – 11.5k cal a BP; G1) within

MIS 2. Each event shows high MS, mean grain size values, and high gravel and low sand contents (Fig. 4). The exclusive presence of gravel ($>2\text{mm}$; Fig. 4) and fresh, flat-surfaced macroscopic pink granite clasts of varying dimensions (~ 2 – 5 cm diameter; Fig. 6, supporting Figs S1 and S2) during these events demonstrates their formation either by glacial abrasion, a common mechanical weathering process of provenance rocks under cold climatic conditions, and/or their delivery through hill-slope processes such as mass wasting and landsliding from the nearby Yin Mountains composed of crystalline granite and gneisses and sedimentary rocks. Strikingly, these two G events are separated by gravel-free sediments with low MS values but high sand and silt contents at ~ 1125 – 965 cm (Fig. 4), corresponding to about 21.8–19.1k cal a BP. This interval closely correlates with the global Last Glacial Maximum (LGM, $21 \pm 2\text{k}$ cal a BP; Mix *et al.*, 2001). Figure 4 shows the internal complexity within G1 and G2. For instance, G1 is characterized by three depositional phases (1a, 1b and 1c) with high MS, mean grain size values, and gravel content centred at ~ 14.3 , 15.7 and 17.1k cal a BP. Likewise, three peaks of G2 (2a, 2b and 2c) are centred at ~ 22.2 , 24 and 25.2k cal a BP. Closer examination of proxy records along with core photographs reveals three granite clast layers (GL1, 2 and 3 in supporting Figs S1 and S2, Table S1) with gravel at narrow depths of ~ 570 – 610 , 760–810 and 1230–1260 cm, corresponding to about 15–15.9, 17–17.3 and 23.5–24k cal a BP.

To determine whether the angular granite clasts are indicative of glacial erosion and/or were delivered by hill-slope mass wasting and landsliding, we undertook microscopic investigations. Petrological microscopic observation of the coarse fraction ($>150\ \mu\text{m}$) from these G events revealed the predominance of light-coloured quartz and pink feldspars as well as numerous dark, opaque specks of magnetite. Fresh surfaces of all minerals with large numbers of sub-angular quartz grains further confirmed physical disintegration by glacial forces rather than from hill-slope processes. SEM analysis of quartz grains from these events indicates surface morphological features of conchoidal and arc-step fractures as well as parallel striations (Fig. 6), diagnostic of mechanical breakage and sculpting of quartz grains beneath glaciers (Morgolis and Krinsley, 1974; Higgs, 1979). Helland and Holmes (1997) demonstrated the presence of parallel striations through SEM investigation on the $>125\text{-}\mu\text{m}$ fraction of sediments from Ocean Drilling Program (ODP) Site 918, off the south-east coast of Greenland. Likewise, Tripathi *et al.* (2008) noted the presence of 10–20% parallel striations from frequency distributions of mechanical textures of glacial origin for $>125\text{-}\mu\text{m}$ grains in sediments from ODP Site 913, Greenland Sea.

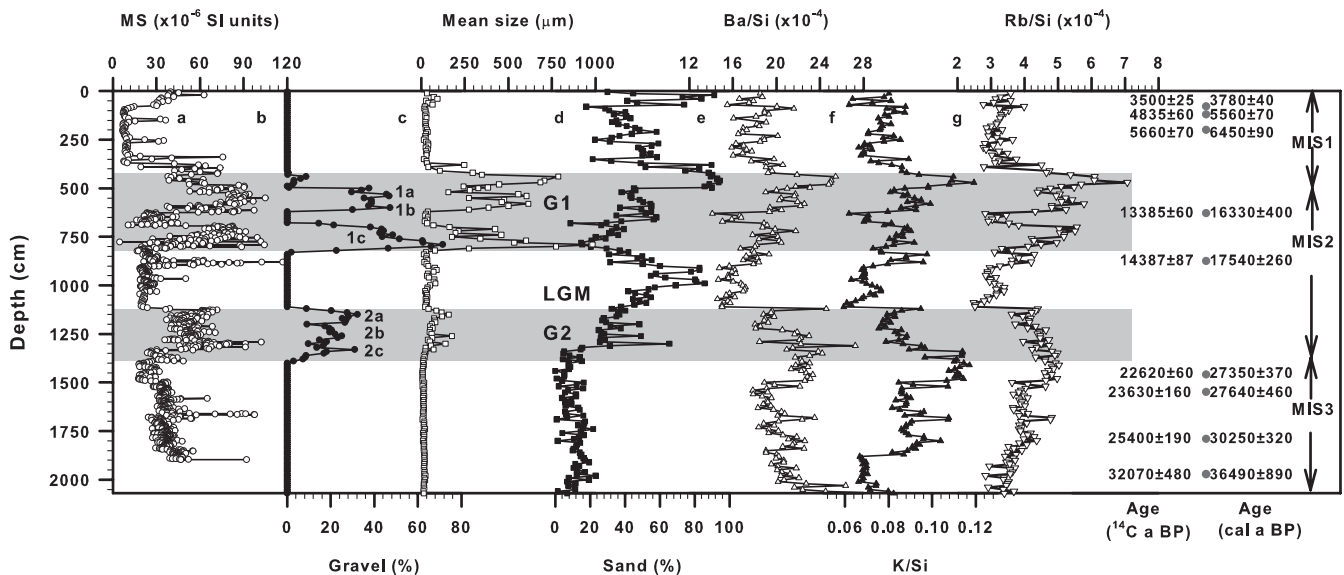


Figure 4. Values of (a) magnetic susceptibility, (b) percentage gravel, (c) mean size, (d) percentage sand, (e) silica-normalized Ba, (f) K and (g) Rb in core WO-1 as a function of depth. Grey bars represent glacially derived sedimentation events G1 and G2 in Inner Mongolia. Dots show raw ^{14}C dates and their calibrated calendar ages. Also shown are climatic boundaries with reference to marine isotope stages (MIS) 1 (10.6k cal a BP–present), 2 (26.2–10.6k cal a BP) and 3 (~40–26.2k cal a BP). LGM, Last Glacial Maximum.

SEM-EDX spot analysis of hand magnet-separated black specks confirmed the dominance of magnetite, titanomagnetite and ilmenite (Table 2), which are responsible for the very high MS values during these two G events. A two-fold increase of silica-normalized large ion lithophile (LIL) elements Ba, K and Rb in G1 and G2 (Fig. 4) is consistent with enhanced detrital sediment delivery from granite rocks rich in Fe–Ti minerals. Incipient chemical index of alteration (CIA) values of 41–58 calculated as in Selvaraj and Chen (2006) were very close to the upper continental crust (CIA = 46). The CIA as well as high Rb/Sr_{det} ratios (supporting Appendix S2: Detrital strontium–Sr_{det} and Fig. S3) are probably due to enhanced physical erosion of K-feldspar-rich pink granite and a lack of chemical weathering

in the organic acid-free provenance (TOC = ~0.2%) dominated by glaciers in the source region.

Discussion

Deglacial events and LGM in Inner Mongolia

An important issue in the reconstruction of glacial activity is the timing between the deposition of glacially derived material and glacial advance and retreat (Owen *et al.*, 2002). The absence of both gravel and granite clasts in sediments of LGM age suggest that glaciers covered provenance rocks at their maximum extent and in turn insignificant meltwater flow was reported in central Asia within MIS 2 (Gillespie and Molnar, 1995). This also implies that glacially derived materials were probably delivered to the lake by episodic meltwater discharge from the Yellow River. Immediately after the G2 interval, the gravel content decreases to zero in the lake core at ~21.5k cal a BP. Sediment at ~1035–1125 cm is dominated by sandy silt and silty sand without gravel or granite clasts (see supporting Table S1). Dry cracks with a random orientation and cracked sandy silt/silty sand deposits (supporting Fig. S2) mark their formation. It may thus be a possible indicator of LGM culmination in the study region, as the corresponding age of 21.8–20.2k cal a BP lies within the age of 26 and 20k cal a BP during which networks of thermal-contraction frost cracking due to a mean annual temperature ~13°C lower than today was reported for the Ordos Plateau (Vandenberghe *et al.*, 2004). Vandenberghe *et al.* (2004) also noted the occurrence of ice-wedge pseudomorphs and sand wedges, indicators of permafrost, in their study area. The presence of such periglacial features confirms the occurrence of continuous permafrost in Inner Mongolia even south of 38°N during the LGM.

By contrast, the gravel content increases sharply to 70% at ~830 cm. Here the highest number of granite clasts (GL2 in supporting Fig. S1) and gravel were deposited rapidly as a ~160-cm-thick sediment sequence, corresponding to about 17.3–17k cal a BP. This implies the onset of deglaciation on the Tibetan plateau, with glacial retreat at ~17.3k cal a BP when there was a major recession of continental mountain glaciers in both hemispheres (Denton *et al.*, 1999; Schaefer *et al.*, 2006).

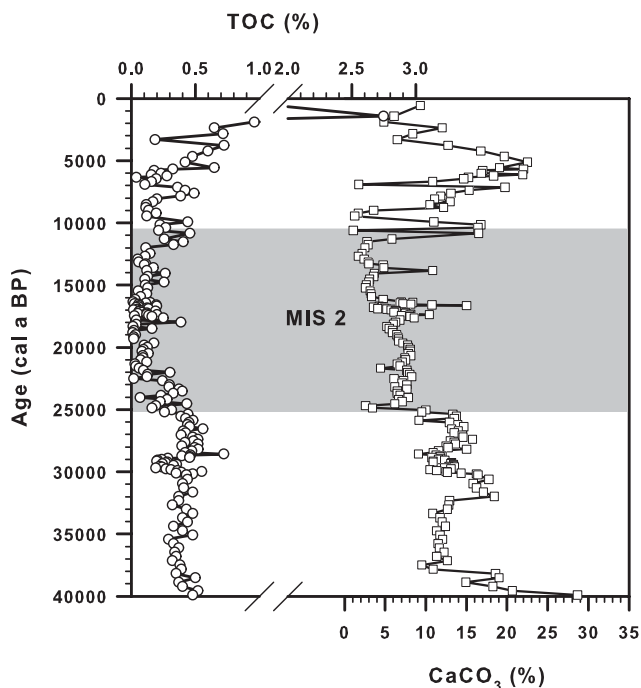


Figure 5. TOC and CaCO₃ contents in core WO-1 as a function of calendar age. Grey shaded region marks the interval of Marine Isotope Stage (MIS) 2.

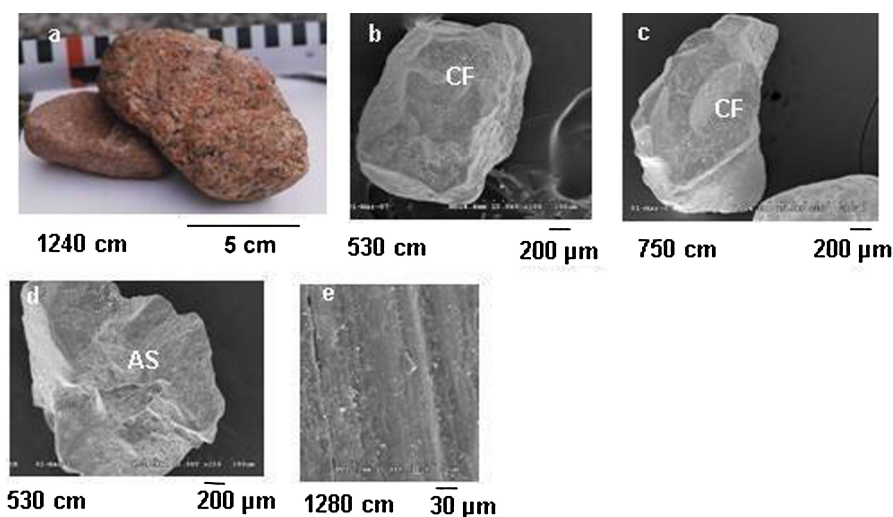


Figure 6. (a) Photograph of fresh granite clast recovered from the G2 interval. (b–e) Scanning electron microphotographs of quartz grains from glacially derived sedimentation events showing surface microfeatures of (b,c) conchoidal fractures (CF), (d) arc-step fractures (AS) and (e) striations, all characteristic of glacial activity. Respective depths (in cm) and image sizes are also given. This figure is available in colour online at wileyonlinelibrary.com.

The highest number of granite clasts correlates with the commencement of mid-latitude deglaciation based on the mean age (17.3k cal a BP) of surface exposure and ^{14}C dating of moraines and glacial deposits (Schaefer *et al.*, 2006). This demonstrates that the greatest meltwater discharge, probably in association with rafts of icebergs and stronger flow in the Yellow River, occurred during the last deglaciation, a finding that correlates well with the deglacial warming of Antarctica and the rise of atmospheric CO_2 content (Monnin *et al.*, 2001). While considering the 1σ error of our calendar ages, we may tentatively fix the LGM termination in Inner Mongolia at ~ 17 – 17.7 k cal a BP. A prominent MS peak at ~ 19.1 k cal a BP suggests a meltwater episode and, by extension, indicates the initial melting of Tibetan glaciers after the LGM. This timing appears to match the sea surface temperature-indicated deglacial warming in the subtropical Pacific (19 ± 1 k cal a BP; Kiefer and Kienast, 2005).

Provenance

Granite clasts, gravel, and high-specific-gravity (5.17 and 5.18) magnetite in G1 and G2 probably originated either from mountains containing pink granite in Qilianshan (max. altitude 5827 m a.s.l.; Fig. 1) or the Yin Mountains composed of ancient crystalline granites and gneisses and sedimentary rocks. The Qilian Mountains are located ~ 1000 km upstream of the study area, and in this region widespread glacial advances and retreats were reported during MIS 2 (Lasserre *et al.*, 2002; Owen *et al.*, 2003). During the LGM, glaciers probably advanced to lower altitudes in the Qilian Mountains, similar to advances that transported moraines to lower altitudes in the Karakoram Mountains (Owen *et al.*, 2002). These reworked glacier-derived sediments stabilized when glacial retreat started at ~ 17.3 k cal a BP after maximum glacial advancement during the LGM. This

timing corresponds to deglaciation from increased summer insolation, which produces copious meltwater that pushes glacier-grinded materials downslope to the Yellow River and, finally, the lake site. Reduced glacial erosion prior to the LGM seems to be responsible for the fewer granite clasts and low gravel content during G2. SEM-EDX reveals the unique presence of strongly magnetized magnetite- Fe_3O_4 in GL1, but weakly magnetized ilmenite- FeTiO_3 and titanomagnetite in GL2 and GL3 (Table 2 and supporting Figs S1 and S2). Such distinct mineralogical differences are responsible for the high and low MS values, respectively, of these sediments. These differences also support the internal complexity of G1 and G2 sedimentation events. Although this implies different source rocks for sediments of G1 and G2, the low altitude (< 2300 m a.s.l.) of nearby mountains (Langshan, Helanshan and Yinshan shown in Fig. 1) makes them less likely sources of glacially derived materials.

However, the Yin Mountains have the lowest slope and mean relief, similar to values for the Helishan and Langshan Mountains, all of which are probably at an early stage of orogenesis (Palumbo *et al.*, 2009, 2011). Palumbo *et al.* (2009) demonstrated lithological control on denudation rates in these mountains based on ^{10}Be concentrations of quartz grains from stream sediments. As larger grains are more rapidly exhumed by mass wasting than smaller grains, ^{10}Be concentration in the 4–8-mm size fraction was about five times lower than in 0.125–0.25- and 0.25–0.50-mm fractions. Sedimentary transport on the hill-slopes of these mountain catchments is currently controlled by surface wash, creep and dry ravel, which results in coarser sediment grain sizes in the channels that are generally below 10 cm (Palumbo *et al.*, 2011). Given that the Yin Mountains are primarily composed of ancient crystalline granite and gneisses and sedimentary rocks (Fig. 1), the intermittent occurrence of granite clasts in core WO-1 may also

Table 2. Results of energy dispersive X-ray (EDX) spot analysis of black particles from glacially derived sedimentation events showing the dominant presence of magnetite in GL1 and titanomagnetite and ilmenite in GL2 and GL3 intervals.

| Depth interval (cm) | Si (%) | Al (%) | Ti (%) | Fe (%) | O (%) | Ca (%) | Mg (%) | Na (%) | Mn (%) |
|---------------------|--------|--------|--------|--------|-------|--------|--------|--------|--------|
| 550–570 | 1.34 | – | – | 75.50 | 23.16 | – | – | – | – |
| | 1.27 | 0.77 | – | 74.49 | 23.47 | – | – | – | – |
| | 2.45 | 1.75 | – | 71.09 | 24.71 | – | – | – | – |
| 750–760 | 6.77 | 3.22 | 26.75 | 24.04 | 36.68 | 1.11 | 1.51 | – | – |
| | 6.13 | 2.95 | 6.20 | 52.12 | 30.11 | 0.84 | 1.66 | – | – |
| | 5.32 | 1.89 | 6.72 | 51.41 | 29.29 | 4.69 | 0.70 | – | – |
| 1240–1250 | 2.76 | 1.39 | 26.62 | 33.14 | 33.00 | – | 1.04 | 1.17 | 0.89 |

suggest that hill-slope mass wasting and landsliding in the Yin Mountains are alternative sources for granite clasts into the lake. Consistent with this, a sediment core recovered from Koucha Lake in the north-eastern Tibetan Plateau shows a thin gravel layer with a maximum grain size of 13 mm, which Mischke *et al.* (2008) attributed to a flash flood triggered by an exceptional rainfall event. Additional evidence for the Yin Mountains as a possible source of granite clasts comes from studies on groundwater arsenic (As) pollution in the Hetao region, which suggest that the heavy metal content in water and soil decreases gradually with increasing distance from the ore deposit zone fronting the Yin Mountains in the upper reaches of the Hetao plain (Zhang *et al.*, 2002; Zhang, 2004). Zhang *et al.* (2002) also found that the groundwater isotopic ratios of $^{87}\text{Sr}/^{86}\text{Sr}$, $^{206}\text{Pb}/^{204}\text{Pb}$ and $^{207}\text{Pb}/^{204}\text{Pb}$ of the most contaminated area are close to the isotopic ratios of mine water rather than of the water used for irrigation from the Yellow River.

In contrast to MIS 2, sediments of clayey silt (77–99%) deposited between ~40 and 26.2k cal a BP during MIS 3 in Wuliangshai Lake indicate an overall warm and wet climate. High MS values coincide with comparatively low values of silica-normalized LIL elements but relatively high CIA values (60–70; Fig. 1 and supporting Fig. S3), which indicates increased precipitation, moderate chemical weathering and active pedogenesis resulting from mild summer insolation and unusually high normal winter insolation during MIS 3 (Feng *et al.*, 2007). Sediments deposited during MIS 1 show the lowest MS values caused by the deposition of loess-like materials, which indicates a dry climate with weak monsoons (Figs 4 and 7). The transition from gravel-bearing sands to silt-dominated sands at ~10.6k cal a BP suggests that the lake was probably detached from the Yellow River around the beginning of the Holocene, when meltwater input from mountain glaciers was reduced, although the East Asian summer monsoon had increased substantially in arid China (An *et al.*, 2000).

Climatic links

The time intervals of G2 and G1 correspond to the formation of Malan loess layers PL3 (24.1–22.6k cal a BP) and PS1 (17.2–14.4k cal a BP) as a result of a stronger winter monsoon in central China (Chen *et al.*, 1997). Based on ^{10}Be and ^{26}Al dating on moraine materials from the Karakoram Mountains of northern Pakistan, Owen *et al.* (2002) observed two glacial advances in MIS 2 at ~25–21 and ~18–15k cal a BP during periods with a weak summer monsoon in south-west Asia. Our glacier-derived sedimentation events roughly correlate with these glacial advances, thereby suggesting the possibility of glacial ice discharge in the Yellow River during intervals of strong winter and weak summer Asian monsoons during MIS 2. Consistent with this hypothesis is the observation that the timing calculated for our glacially derived deposit intervals match the timing of weak summer monsoons indicated by low negative $\delta^{18}\text{O}$ values reported for stalagmites from caves in eastern China (Wang *et al.*, 2001; Yuan *et al.*, 2004) (Fig. 7).

Interestingly, the ages of GL1 (15–15.9k cal a BP), GL2 (17–17.3k cal a BP) and GL3 (23.5–24k cal a BP) roughly correspond to H1 and H2, when greater amounts of lithic grains were discharged into the North Atlantic by massive icebergs (Bond *et al.*, 1997) (Fig. 7). Such coincidence implies the possibility of rafts of icebergs in the Yellow River along with suddenly released meltwater discharges, similar to ice-rafts into the North Atlantic during Heinrich events. Although there is no increase in gravel or granite clasts, the MS peak at ~28.9–29.2k cal a BP (CS1 in Fig. 7 and supporting Table S1) with >20% of very coarse sand (>1 mm) during MIS 3 represents a

meltwater pulse that apparently corresponds with H3. The MS time series shows high values at ~15.4–12.9k cal a BP, corresponding to a warm, Bølling-Allerød interstadial. The coeval increase of gravel and mean grain size indicates increased meltwater discharge in the Yellow River. With the return to a relatively cold stadial, MS shows a decreasing trend at ~12.8–11.6k cal a BP that probably correlates with the Younger Dryas in the North Atlantic (Fig. 7). These MS-related inferences are further substantiated by silica-normalized LIL elements showing high and low values during these events (Fig. 4), confirming enhanced detrital discharge during the warm Bølling-Allerød event.

The effect of iceberg discharge is thought to be restricted to the North Atlantic between 40° and 50°N (Ruddiman, 1977; Grousset *et al.*, 1993). A study of a sediment core (SU8118) from outside the IRD belt in the Iberian margin (37°46'N), however, shows an increase in the percentage of IRD and MS values during two periods (23–26 and 18–15.5k cal a BP) of low sea surface temperatures (Bard *et al.*, 2000). Our combined panel, including IRD and MS data (Fig. 7), reveals a close correlation with granite clast layers, suggesting the possibility of mountain glacial advances during the time intervals of low sea surface temperatures in the North Atlantic. Figure 7 shows the correlation of GL1 and GL2 in core WO-1 with the twinned IRD peaks of H1 (1a, 16k cal a BP; 1b, 17.5k cal a BP) in core SU8118. Likewise, GL3 and gravel peak 2c appear to coincide with the two depositional phases of H2 (2a, 23.5k cal a BP; 2b, 25k cal a BP). Such a remarkable resemblance, including small-scale changes, of glacially derived sedimentation events in arid Inner Mongolia with Heinrich events in the North Atlantic suggests that North Atlantic cooling and the strengthening of the Asian winter monsoon exert strong controls on mountain glaciers, and therefore on detrital material delivery by the Yellow River to the lake studied.

Conclusions

We have demonstrated that distinct climatic conditions prevailed during MIS 2 in arid Inner Mongolia through dating of physical and geochemical sedimentary records of Wuliangshai Lake. Proxy records identified the presence of detrital moraine deposits during two intervals, G2 (26.2–21.8k cal a BP) and G1 (17.3–11.5k cal a BP), indicating the influence of mountain glaciers on Yellow River discharge during MIS 2. Numerous granite clasts, gravel and a higher amount of magnetite along with high ratios of silica-normalized LIL elements support physical weathering of source rocks beneath glaciers and transportation of glacially derived materials through the Yellow River and/or sediment influx through hill-slope mass wasting and landsliding from the nearby Yin Mountains, composed of ancient crystalline granites and gneisses and sedimentary rocks. The time intervals of glacially derived sedimentation matches with the formation of loess layers in Malan Loess, glacial advances in the Himalayas, and a weak summer monsoon in eastern China and Heinrich events in the North Atlantic. Our study allows us to speculate on the existence of glacial ice along the course of the Yellow River at least during the events of G2 and G1, consistent with iceberg discharge away from the ice-rafted belt observed in the Iberian margin by Bard *et al.* (2000). Although the climatic link shown here suggests that continental glaciers up to 40°N appear to behave coherently with glaciers at high latitudes, based on our records alone, we cannot determine whether glacially derived materials were transported largely by meltwater pulses associated with glacial retreat or were rolled-down from the Yin Mountains through hill-slope mass wasting and landsliding. The link proposed between granite clast layers in Wuliangshai

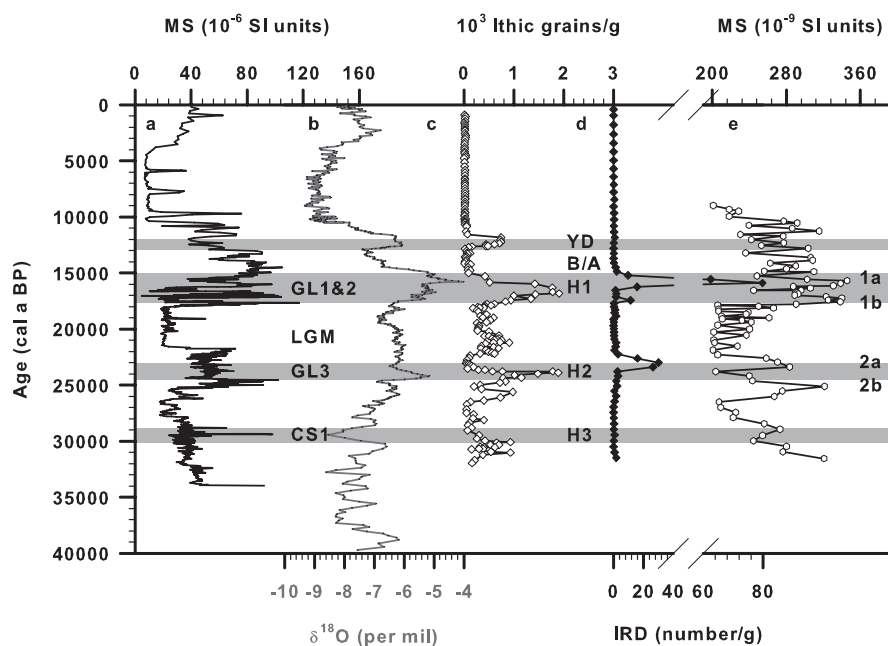


Figure 7. Layers of granite clasts (GL1, 2, 3) and very coarse sand (CS1) in Inner Mongolia combined with records of East Asian monsoon and Heinrich (H) events in the North and North-east Atlantic. (a) MS values in core WO-1 as a function of calendar age, (b) $\delta^{18}\text{O}$ records of Hulu and Dongge caves (Wang *et al.*, 2001; Yuan *et al.*, 2004), (c) number of lithic grains (Bond *et al.*, 1997), (d) ice-rafted debris and (e) MS data of Bard *et al.* (2000). YD, Younger Dryas; B/A, Bølling-Allerød.

Lake and Heinrich events in the North Atlantic seems to be consistent with a previous study from the western loess plateau that found evidence for Heinrich events based on grain size and calcium carbonate variations (Chen *et al.*, 1997). However, the chronology of our record does not allow us to confirm this particular link and the tentative link interpreted in this study warrants further high-resolution, well-dated records from the Hetao Plain for critical evaluation. Regardless, our data provide the first evidence for the influence of glacier-derived sedimentation in arid Inner Mongolia.

Supporting information

Additional supporting information can be found in the online version of this article:

Fig. S1. Photographs of core WO-1 and demarcation of glacially derived sedimentation events, granite clasts layers and Last Glacial Maximum interval.

Fig. S2. A layer at ~1125–1035 cm.

Fig. S3. Chemical index of alteration and Rb/Sr_{det} ratio.

Table S1. Lithostratigraphy of core WO-1.

Appendix S1. Chronology.

Appendix S2. Detrital strontium-Sr_{det}.

Please note: This supporting information is supplied by the authors, and may be re-organized for online delivery, but is not copy-edited or typeset by Wiley-Blackwell. Technical support issues arising from supporting information (other than missing files) should be addressed to the authors.

Acknowledgements. We thank the National Science Council for financial support of Taiwan (NSC 95-2811-Z-110-002, 95-2621-Z-110-005 and 95-2621-M-110-001), the National Science Foundation of China (No.: 41176059 and 41121091) and the TOP University Program (00C 0302 02), also Y. H. Shau for access to SEM, and P. M. Grootes for age model discussion. We thank Jim Rose and one anonymous reviewer for their constructive comments that greatly improved the manuscript.

Abbreviations. CIA, chemical index of alteration; IC, inorganic carbon; IRD, ice-rafted debris; LGM, Last Glacial Maximum; LIL, large ion lithophile; MIS, Marine Isotope Stage; MS, magnetic susceptibility; pMC, percentage modern carbon; SEM-EDX, scanning electron microscopy-energy dispersive X-ray; TC, total carbon; TOC, total organic carbon.

References

- An ZS, Porter SC., 1997. Millennial-scale climatic oscillations during the last interglaciation in central China. *Geology* **25**: 603–606.
- An ZS, Porter SC, Kutzbach JE, *et al.* 2000. Asynchronous Holocene optimum of the East Asian monsoon. *Quaternary Science Reviews* **19**: 743–762.
- Bard E, Rostek F, Turon J-L., *et al.* 2000. Hydrological impact of Heinrich events in northeast Atlantic. *Science* **289**: 1321–1323.
- Benson LV, Burdett JW, Kashgarian M, *et al.* 1996. Climatic and hydrologic oscillations in the Owens Lake Basin and adjacent Sierra Nevada, California. *Science* **274**: 746–749.
- Bond, GC, Broecker W, Johnsen S, *et al.* 1993. Correlations between climate records from North Atlantic sediments and Greenland ice. *Nature* **365**: 143–147.
- Bond GC, Showers W, Cheseby M, *et al.* 1997. A pervasive millennial-scale cycle in North Atlantic Holocene and glacial climates. *Science* **278**: 1257–1266.
- Chen FH, Bloemendal J, Wang JM, *et al.* 1997. High-resolution multi-proxy climate records from Chinese loess: evidence for rapid climatic changes over the last 75 kyr. *Palaeogeography, Palaeoclimatology, Palaeoecology* **130**: 323–335.
- Chen FH, Fan YX, Chun X, *et al.* 2008. Preliminary research on Megalake Jilantai-Hetao in the arid areas of China during the Late Quaternary. *Chinese Science Bulletin* **53**: 1725–1739.
- Danzeglocke U, Jöris O, Weninger B., 2008. CalPal^{online} 1.5, available from <http://www.calpal.online.de>.
- Denton, GH, Heusser CJ, Lowell TV, *et al.* 1999. Interhemispheric linkage of paleoclimate during the last glaciation. *Geografiska Annaler Series* **81A**: 105–153.
- Feng ZD, Tang LY, Ma YZ, *et al.* 2007. Vegetation variations and associated environmental changes during marine isotope stage 3 in the western part of the Chinese Loess Plateau. *Palaeogeography, Palaeoclimatology, Palaeoecology* **246**: 278–291.
- Gillespie A, Molnar P., 1995. Asynchronous maximum advances of mountain and continental glaciers. *Reviews of Geophysics* **33**: 311–364.
- Grousset FE, Labeyrie L, Sinko JA, *et al.* 1993. Patterns of ice-rafted detritus in the glacial North Atlantic (40–55°N). *Paleoceanography* **8**: 175–192.
- Guo H, Tang X, Yang S, *et al.* 2008. Effect of indigenous bacteria on geochemical behavior of arsenic in aquifer sediments from the Hetao Basin, Inner Mongolia: Evidence from sediment incubations. *Applied Geochemistry* **23**: 3267–3277.

- Heinrich H., 1988. Origin and consequences of cyclic ice rafting in the northeast Atlantic Ocean during the past 130,000 years. *Quaternary Research* **29**: 143–152.
- Helland PE, Holmes MA., 1997. Surface textural analysis of quartz sand grains from ODP Site 918 off the southeast coast of Greenland suggests glaciation of southern Greenland at 11 Ma. *Palaeogeography, Palaeoclimatology, Palaeoecology* **135**: 109–121.
- Higgs R., 1979. Quartz-grain surface features of Mesozoic–Cenozoic sands from the Labrador and western Greenland continental margins. *Journal of Sedimentary Petrology* **49**: 599–610.
- Kiefer T, Kienast M., 2005. Patterns of deglacial warming in the Pacific Ocean: a review with emphasis on the time interval of Heinrich event 1. *Quaternary Science Reviews* **24**: 1063–1081.
- Lasserre C, Gaudemer Y, Tapponnier P, et al. 2002. Fast late Pleistocene slip rate on the Leng Long Ling segment of the Haiyuan fault, Qinghai, China. *Journal of Geophysical Research* **107**: 2276–2291.
- Mischke S, Kramer M, Zhang C, et al. 2008. Reduced early Holocene moisture availability in the Bayan Har Mountains, northeastern Tibetan Plateau, inferred from a multi-proxy lake record. *Palaeogeography, Palaeoclimatology, Palaeoecology* **267**: 59–76.
- Mix AC, Bard B, Schneider R., 2001. Environmental processes of the ice age: land, oceans, glaciers (EPILOG). *Quaternary Science Reviews* **20**: 627–657.
- Monnin E, Indermühle A, Dällenbach A, et al. 2001. Atmospheric CO₂ concentrations over the last glacial termination. *Science* **297**: 112–114.
- Morgolis SW, Krinsley DH., 1974. Processes of formation and environmental occurrence of microfeatures on detrital quartz grains. *American Journal of Science* **274**: 449–464.
- Owen LA, Finkel RC, Caffee MW, et al. 2002. Timing of multiple glaciations during the Late Quaternary in the Hunza Valley, Karakoram Mountains, Northern Pakistan: defined by cosmogenic radionuclide dating of moraines. *Geological Society of America Bulletin* **114**: 593–604.
- Owen LA, Spencer JQ, Haizhou M, et al. 2003. Timing of Late Quaternary glaciation along the southwestern slopes of the Qilian Shan, Tibet. *Boreas* **32**: 281–291.
- Palumbo L, Hetzel R, Tao M, et al. 2009. Topographic and lithologic control on catchment-wide denudation rates derived from cosmogenic ¹⁰Be in two mountain ranges at the margin of NE Tibet. *Geomorphology* **117**: 130–142.
- Palumbo L, Hetzel R, Tao M, et al. 2011. Catchment-wide denudation rates at the margin of NE Tibet from in situ-produced cosmogenic ¹⁰Be. *Terra Nova* **23**: 42–48.
- Porter SC, An ZS., 1995. Correlation between climate events in the North Atlantic and China during the last glaciation. *Nature* **375**: 305–308.
- Reynolds RL, Rosenbaum JG, Rapp J, et al. 2004. Record of late Pleistocene glaciation and deglaciation in the southern Cascade Range. I. Petrological evidence from lacustrine sediment in Upper Klamath Lake, southern Oregon. *Journal of Paleolimnology* **31**: 217–233.
- Ruddiman WF., 1977. Late Quaternary deposition of ice-rafted sand in the sub-polar North Atlantic (lat. 40° to 60°). *Geological Society of America Bulletin* **88**: 1813–1821.
- Ruth U, Bigler M, Röthlisberger R, et al. 2007. Ice core evidence for a very tight link between North Atlantic and east Asian glacial climate. *Geophysical Research Letters* **34**, L03706. DOI: 10.1029/2006GL027876
- Schaefer JM, Denton GH, Barrell DJA, et al. 2006. Near-synchronous interhemispheric termination of the Last Glacial Maximum in mid-latitudes. *Science* **312**: 1510–1513.
- Selvaraj K, Chen CTA., 2006. Moderate chemical weathering of subtropical Taiwan: Constraints from solid-phase geochemistry of sediments and sedimentary rocks. *Journal of Geology* **114**: 101–116.
- Shi YF., 1992. Glaciers and glacial geomorphology in China. *Zeitschrift fuer Supplement Band* **86**: 51–63.
- Shi YF., 2002. Characteristics of late Quaternary monsoonal glaciation on the Tibetan Plateau and in East Asia. *Quaternary International* **97–98**: 79–91.
- Stuvier M, Reimer PJ, Bard E, et al. 1998. INTCAL 98 Radiocarbon age calibration, 24,000–0 cal B. P. *Radiocarbon* **40**: 1041–1083.
- Sun B, Li C, Zhu D., 2011. Changes in Wuliangsu Lake in past 150 years based on 3S technology. In *International Conference on Remote Sensing, Environment and Transportation Engineering: IEEE Conference Publications*, 24–26, June 2011, Nanjing, China: 2993–2997, DOI: 10.1109/RSETE.2011.5964944.
- Tripathi AK, Eagle RA, Morton A, et al. 2008. Evidence for glaciation in the Northern Hemisphere back to 44 Ma from ice-rafted debris in the Greenland Sea. *Earth and Planetary Science Letters* **265**: 112–122.
- Vandenbergh J, Cui ZJ, Zhao L, et al. 2004. Thermal-contraction-crack networks as evidence for Late-Pleistocene permafrost in Inner Mongolia, China. *Permafrost and Periglacial Processes* **15**: 21–29.
- Wang YJ, Cheng H, Edwards RL, et al. 2001. A high-resolution absolute-dated late Pleistocene monsoon record from Hulu Cave, China. *Science* **294**: 2345–2348.
- Yuan D, Cheng H, Edwards RL, et al. 2004. Timing, duration and transitions of the last interglacial Asian monsoon. *Science* **304**: 575–578.
- Zhang H, Ma DS, Hu, XX., 2002. Arsenic pollution in groundwater from Hetao area, China. *Environmental Geology* **41**: 638–643.
- Zhang H., 2004. Heavy-metal pollution and arseniasis in Hetao region, China. *Ambio* **33**: 138–140.